Wettability of eutectic $NaLiCO_3$ salt on magnesium oxide substrates at 778 K

Li, Chuan; Li, Qi; Cao, Hui; Leng, Guanghui; Li, Yongliang; Wang, Li; Zheng, Lifang; Ding, Yulong

DOI:
10.1016/j.apsusc.2018.02.082

Document Version
Peer reviewed version

Citation for published version (Harvard):
Li, C, Li, Q, Cao, H, Leng, G, Li, Y, Wang, L, Zheng, L & Ding, Y 2018, 'Wettability of eutectic $NaLiCO_3$ salt on magnesium oxide substrates at 778 K', *Applied Surface Science*, vol. 442, pp. 148-155. https://doi.org/10.1016/j.apsusc.2018.02.082

Accepted Manuscript

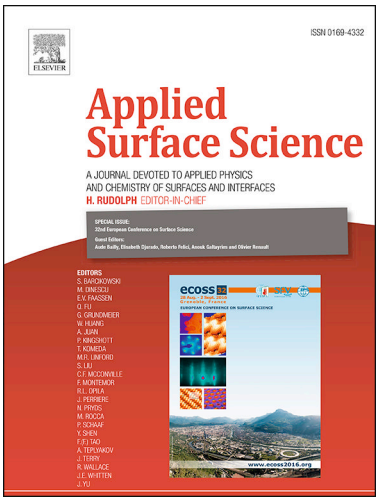

Full Length Article

Wettability of eutectic $NaLiCO_3$ salt on magnesium oxide substrates at 778K

Chuan Li, Qi Li, Hui Cao, Guanghui Leng, Yongliang Li, Li Wang, Lifang Zheng, Yulong Ding

PII: S0169-4332(18)30425-2
DOI: https://doi.org/10.1016/j.apsusc.2018.02.082
Reference: APSUSC 38540

To appear in: *Applied Surface Science*

Received Date: 19 October 2017
Revised Date: 24 December 2017
Accepted Date: 7 February 2018

Please cite this article as: C. Li, Q. Li, H. Cao, G. Leng, Y. Li, L. Wang, L. Zheng, Y. Ding, Wettability of eutectic $NaLiCO_3$ salt on magnesium oxide substrates at 778K, *Applied Surface Science* (2018), doi: https://doi.org/10.1016/j.apsusc.2018.02.082

Wettability of eutectic $NaLiCO_3$ salt on magnesium oxide substrates at 778K

Chuan Li [a], Qi Li [a], Hui Cao [a], Guanghui Leng [a], Yongliang Li [a], Li Wang [b], Lifang Zheng [b,*], Yulong Ding [a,b*]

[a] Birmingham Centre for Energy Storage (BCES) & School of Chemical Engineering, University of Birmingham, Birmingham B15 2TT, UK

[b] University of Science & Technology Beijing, Beijing 10083, China

Abstract

We investigated the wetting behavior of a eutectic carbonate salt of $NaLiCO_3$ on MgO substrates at an elevated temperature of 778K by measuring contact angle with a sessile drop method. Both sintered and non-sintered MgO were prepared and used as the substrates. The sintered substrates were obtained by sintering compacted MgO powders at 500-1300^{o}C. For comparison purposes, a single crystal MgO substrate was also used in the work. The different sintering temperatures provided MgO substrates with different structures, allowing their effects on salt penetration and hence wettability and surface energy to be investigated. A scanning electron microscope equipped with energy dispersive spectrometry and an atomic force microscope were used to observe the morphology and structures of the MgO substrates as well as the salt penetration. The results showed a good wettability of the carbonate salt on both the sintered and non-sintered MgO substrates and the wettability depended strongly on the structure of the substrates. The non-sintered MgO substrate has a loose surface particle packing with large pores and crevices, leading to significant salt infiltration, and the corresponding contact angle was measured to be 25°. The contact angle of the salt on the sintered MgO substrates increased with an increase in the sintering temperature of the MgO substrate,

and the contact angle of the salt on the single crystal substrate was the highest at ~40°. The effect of the sintering temperature for making the MgO substrate could be linked to the surface energy, and the linkage is validated by the AFM measurements of the adhesion forces of the MgO substrates.

Keywords: Wettability; Eutectic carbonate salt; Magnesium oxide; Contact angle; Surface energy

1. Introduction

Surface wetting and its alternation play an important role in numerous industrial applications. One of such applications is related to the storage of thermal energy using composite phase change materials (CPCMs) [1]-[4], which have a wide range of applications including peak shaving of power grids, effective use of curtailed wind energy, solar thermal power generation, and space heating using distributed domestic storage heaters and centralized district heating networks, to name but a few. A CPCM often consists of a phase change material (PCM) and a shape stabilization material (SSM) [5][6]. A thermal conductivity enhancer (TCE) may also be needed in the formulation if heat transfer becomes a constraint [5]-[7]. Such materials can be fabricated by using the following three methods: (a) physical mixing of milled PCM, SSM and TCE, followed by shaping and finally sintering; (b) physical mixing of milled SSM and TCE, then shaping and sintering, followed by vacuum infiltration of PCM at liquid state; (c) shaping and sintering SSM, followed by vacuum infiltration of liquid PCM containing TCE [8]-[10]. In all these methods, the wettability of liquid PCM on both SSM and TCE at elevated temperatures can play a very important role in the determination of structure, density,

mechanical properties, and thermal properties of the composites. However, little has been found in the literature on this area, which forms the major motivation for this work.

Numerous PCMs exist, which can be divided into two categories of organic and inorganic materials. Examples include fatty acids and paraffin waxes, which are organic and mainly for low temperature applications, and carbonate, nitrate and sulphate salts, which are inorganic and mainly for medium to high temperature applications [5][9]. There are many materials that could be used as SSMs, including diatomite, magnesium oxide, expanded graphite and silicates, to name but a few [11][12]. This work focuses on the use of MgO as SSM and eutectic $LiNaCO_3$ $NaLiCO_3$ salt as PCM for the composite. The rationales behind the choice lie in the high surface energy of MgO towards the carbonate salt and high energy density of the PCM. The main objective is to investigate the wettability of the eutectic carbonate salt of $NaLiCO_3$ on MgO substrates through the measurements of contact angle. The influences of two factors on the contact angle were studied: (a) penetration of carbonate salt into MgO substrate, which may change the contact angle dynamically, and (b) surface tension changes due to different fabrication temperatures of the substrates, for which little information can be found in the literature. Scanning electron microscopy with energy dispersive X-ray spectrometry (SEM-EDS) and atomic force microscopy (AFM) were used in the study.

2. Experimental method

2.1 Preparation of eutectic carbonate salt samples and MgO substrates

The salt samples used in this study were made with eutectic carbonate salt ($NaLiCO_3$), which were in a cylindrical (rod) shape and had a mass of approximately 50 mg. The

eutectic carbonate salt contained 50 wt% Li_2CO_3 and 50 wt% Na_2CO_3. The samples were made by thoroughly mixing the two salts followed by shaping in a cylindrical mould with diameter of 4 mm. MgO substrates used were either a sintered or a non-sintered cylindrical plate with 13 mm diameter and 4 mm thickness. The sintered MgO plates were sintered at different temperature from 500 ℃ to 1300 ℃ to examine the effect of salt infiltration into MgO substrates (substrates sintered at different temperatures give different porosity). For comparison purpose, a 10mm×10mm single crystal MgO (100) plate (Sigma-Aldrich Co. LLC, UK) was purchased, which had a purity of 99.9% and a relative density over 96%. One flat surfaces of the plates was polished to give a mirror finish using various grades of SiC abrasive papers and three grades of diamond pastes (with particle diameters of 6, 3 and 1 μm) to an average surface roughness of 400-500 nm as measured by a surface profilometer (KLA Tencor MicroXAM 2, USA) over a length of 150 μm at a speed of 20 μm/s. The substrates were carefully cleaned in acetone using an ultrasonic machine before wettability experiments.

2.2 Experimental apparatus and measurement methods

A high temperature drop shape analyzer (Krüss, DSAHT17-2, Germany) was used to investigate the wetting behavior of eutectic carbonate salt on MgO substrates. The device is based on the sessile drop method; see Fig. 1 for a schematic illustration and an image of the experimental apparatus.

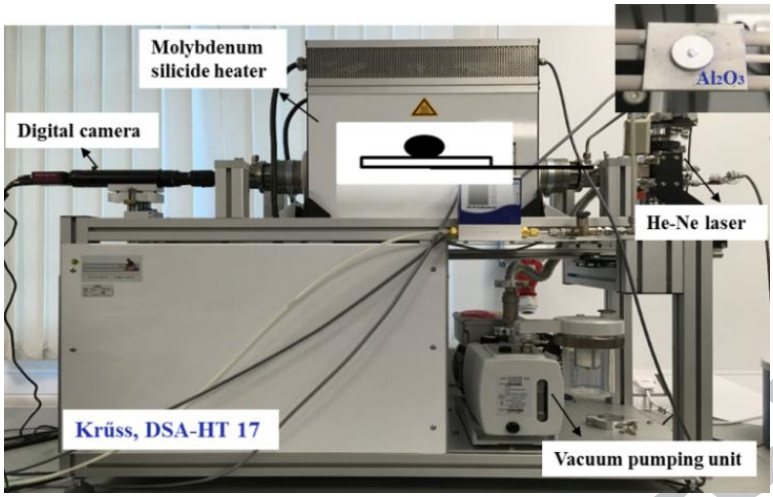

Fig. 1. A schematic illustration and a photograph of the sessile drop test apparatus.

The analyzer consists of a molybdenum reflector installed in a sealed chamber, a molybdenum silicide heater, an aluminum oxide supporting tube and a sample holding platform. It uses a type B thermocouple to measure, monitor and control the temperature through a programmable controller. There is a vacuum pumping unit with a rotary pump and a turbo molecular pump to control the pressure and atmosphere of the sealed chamber. The analyzer is equipped with a high-resolution digital camera providing an angular resolution of 0.1 degree and installed with an analysis software package.

A scanning electron microscope (SEM) with EDS (TM3030, HITACHI, Japan) was used for microstructural observations of the interface between the salt and the substrate. The surface morphology and roughness of the substrates were observed with an atomic force microscope (AFM, NanoWizard III NanoScience, Germany). In a typical experiment, a cylindrical sample was placed on an MgO substrate. The sample-substrate set was then carefully transferred to the holding platform, which upon adjusted to give a horizontal orientation before inserted into the center of the chamber. The chamber was then sealed

followed by purging the chamber with a high purity nitrogen stream while being heated up to a pre-set temperature (505^{o}C, 778K in this work) at a heating rate of 10 K/min. When the sample reached the measurement temperature, the N_2 gas flow was cut off and the digital camera was started to capture the image of the salt sample. The drop analysis software was then used to obtain the contact angle, the sample height and the contact diameter. Each experiment was repeated at least twice to study the repeatability. At end of experiments, the chamber was cooled down and the sample was then taken out for further analyses using the SEM-EDS and AFM.

3. Results and discussion

3.1 Surface roughness of substrates

It is well known that, for a given substrate material and a liquid, the wettability of the liquid on the surface is affected by surface roughness. Wenzel [13][14] studied such an effect and obtained the following relationship:

$$\cos\theta_R = A_R \cos\theta_i \quad (1)$$

where θ_R and θ_i represent respectively the contact angle on rough and smooth surfaces; and the A_R is the ratio of the true area of the rough surface to that of the smooth surface. The Wenzel model indicates that the contact angle of a liquid on a rough surface scales linearly to the surface ratio. Fig. 2 shows the AFM images of different MgO substrates (polished) from which the 3D surface roughness parameters can be calculated and the data are listed in Table 1.

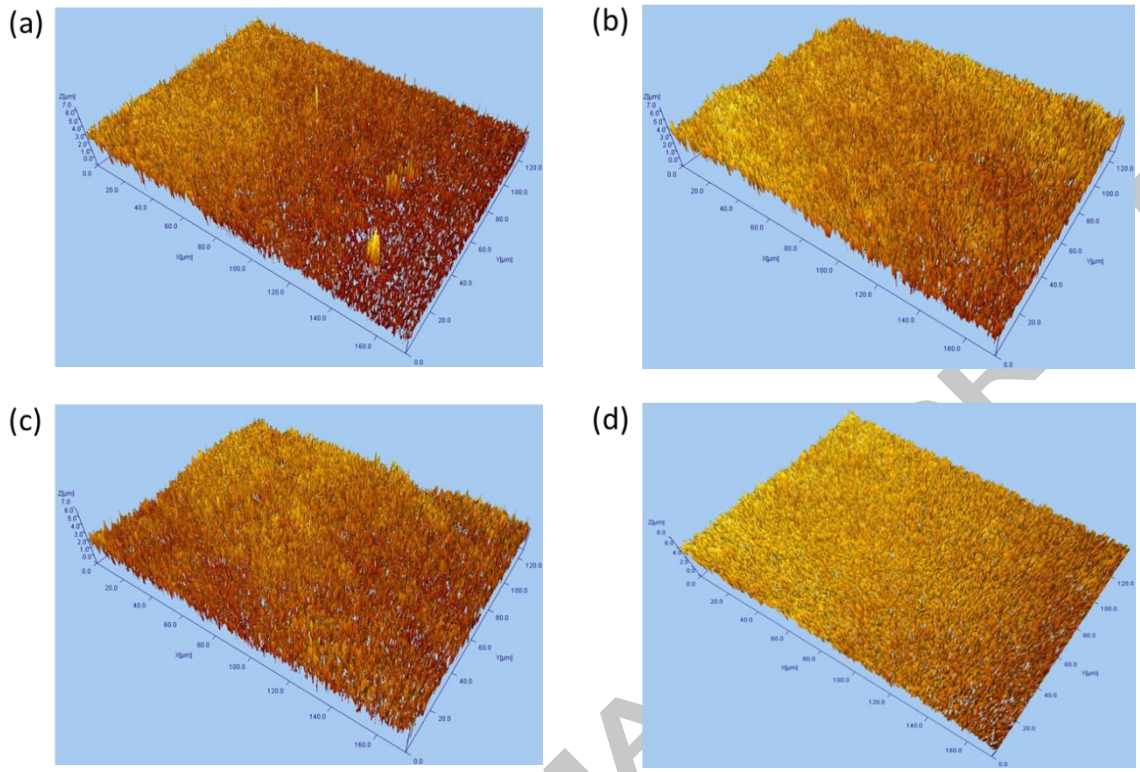

Fig. 2. 3D roughness profiles of MgO substrates: (a) non-sintered, (b) sintered at 500°C, (c) sintered at 1300°C, and (d) single crystal.

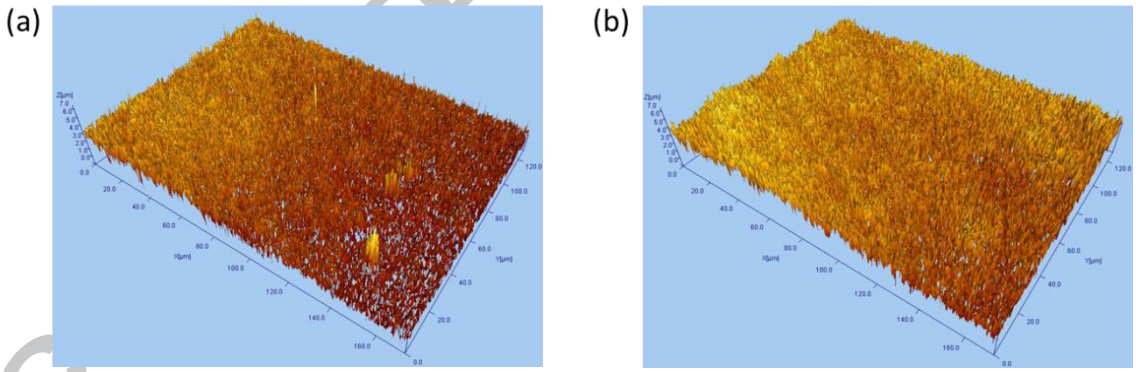

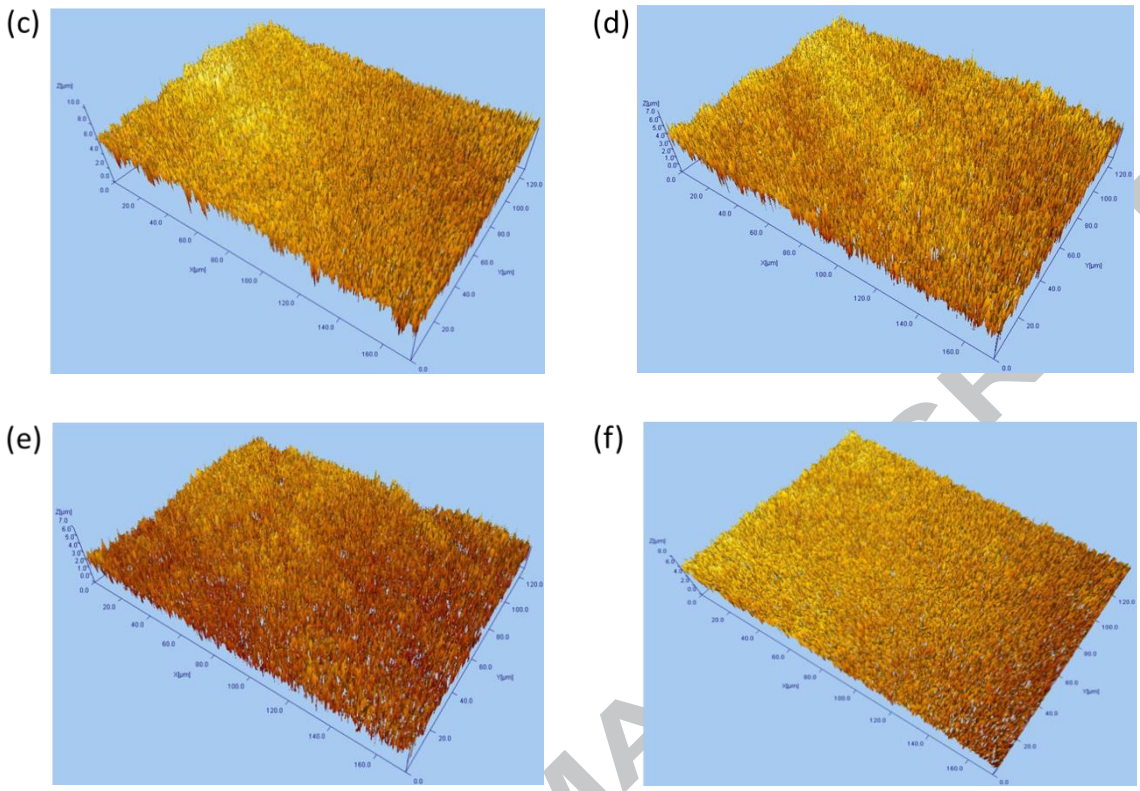

Fig. 2. 3D roughness profiles of MgO substrates: (a) non-sintered, (b) sintered at 500°C, (c) sintered at 900°C, (d) sintered at 1100°C, (e) sintered at 1300°C, and (f) single crystal.

The roughness parameters shown in Table 1 are the average roughness (R_a), the root-mean-square roughness (R_q), the valley depth or maximum height (R_z), the core roughness depth (R_k), and the kurtosis of the roughness (R_{ku}). One can see that all the polished MgO substrates have an average surface roughness of 430-510 nm (first row of Table 1) and therefore the surface roughness is excluded as a variable in the subsequent analyses and discussion.

Table 1

Surface roughness data of the polished MgO substrates obtained from AFM

Parameter	Non-sintered	Sintered at 500 °C	Sintered at 1300 °C	Sintered at 3000 °C

R_a (µm)	0.51	0.496	0.461	0.436
R_q (µm)	0.666	0.623	0.592	0.565
R_z (µm)	5.32	4.92	4.53	4.18
R_k (µm)	2.12	1.9	1.56	1.31
R_{ku} (µm)	2.99	3.25	3.72	4.07

Table 1

Surface roughness data of the polished MgO substrates obtained from AFM

Parameter	R_a (µm)	R_q (µm)	R_z (µm)	R_k (µm)	R_{ku} (µm)
Non-sintered	0.51	0.666	5.32	2.12	2.99
Sintered at 500 °C	0.496	0.623	4.92	1.9	3.25
Sintered at 900 °C	0.483	0.614	4.79	1.79	3.49
Sintered at 1100 °C	0.472	0.608	4.65	1.67	3.61
Sintered at 1300 °C	0.461	0.592	4.53	1.56	3.72
Sintered at 3000 °C (single crystal)	0.436	0.565	4.18	1.31	4.07

3.2 Contact angle and drop dimension measurements

Fig. 3 shows the time evolution of the contact angle (θ) and the droplet diameter (D) and height (H) of the eutectic carbonate salt on the non-sintered MgO substrate at a measurement temperature of 505°C (778K). It can be seen that the contact angle and drop dimension change with time, and the change can be divided into three stages: an initial stage (a), a spreading stage (b), and a steady state stage (c). The initial stage could be regarded as the equilibrium stage since the contact angel and the droplet dimension are almost constant, and the spreading velocity is very low as the salt sample just starts to melt. In the stage (b), both the contact angle and droplet height decrease whilst the

droplet diameter increases, indicating the spreading of droplet on the triple line as carbonate-MgO is a non-reacting system [6][7]. In the stage (c), the contact angle and droplet dimension are almost constant, indicating the constraint of energetic equilibrium on the substrate surface.

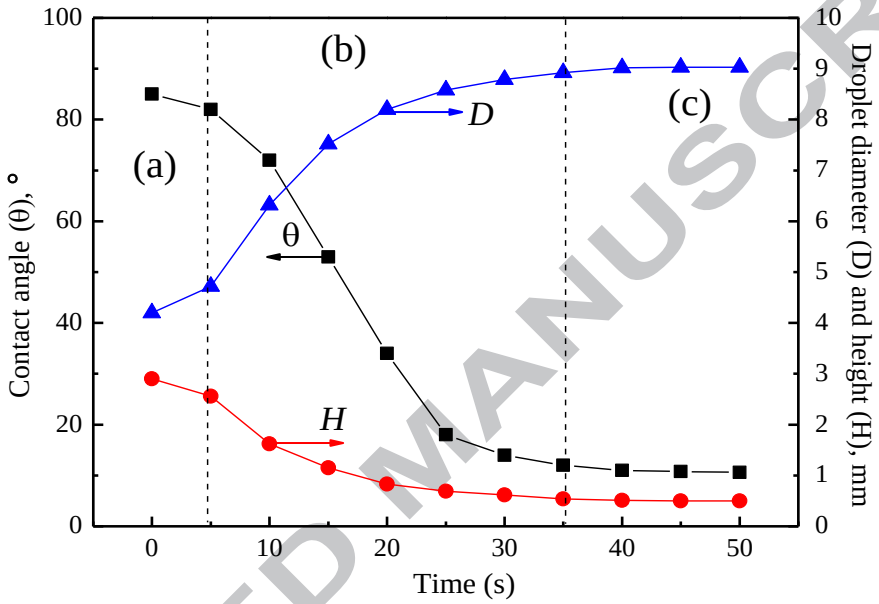

Fig. 3. Time evolution of the contact angle and droplet dimension of carbonate salt on a non-sintered MgO substrate.

Fig. 4 demonstrates the contact angle and droplet dimension of the eutectic salt droplet on the MgO substrate sintered at 1100°C. One can see clearly the three stages of the spreading process, similar to the observations with the salt on the non-sintered MgO substrate. However, the durations of the first two stages are far longer compared with that of the salt on the non-sintered MgO substrate: Stage (a) lasts ~ 8s (~ 5s for the non-sintered case) and Stage (b) is ~ 57s (~ 30s for the non-sintered case). The equilibrium

contact angle approaches ~ 25° (~ 12° for the non-sintered case). These observations indicate that the wettability of eutectic carbonate salt on the sintered substrate is lower than that on the non-sintered substrate. The enhanced wettability is likely due to the salt infiltration into the MgO substrate and surface energy effects of MgO substrate, which will be discussed further in Sections 3.3 and 3.4.

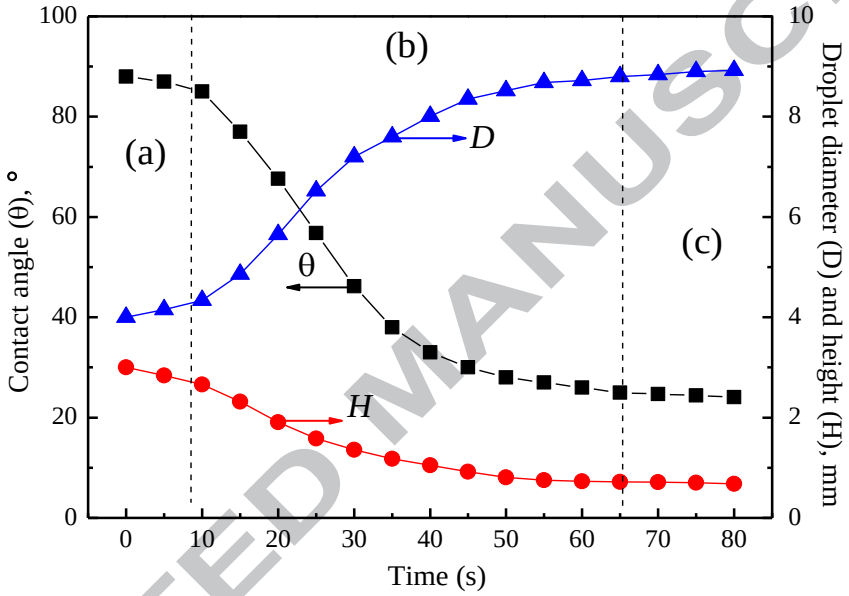

Fig. 4. Time evolution of contact angle and droplet dimension of carbonate salt on an MgO substrate sintered at 1100°C.

3.3 Salt infiltration effect

The salt infiltration was studied by using SEM-EDS as mentioned in Section 3.2. Fig. 5 shows typical top-view SEM images of the non-sintered MgO substrate and the MgO substrate sintered at 1100°C. Far coarser structures / particles are seen on the non-sintered MgO substrate, which are less uniformly distributed, as compared with the sintered

substrate. Although the uniaxial compression and polishing processes were applied during sample preparation, some cavities of ~ 3-5 μm are apparent in the non-sintered substrate (Fig. 5a). Fine particles are seen to distribute uniformly and densely packed on the sintered MgO substrate although there are still some micro crevices with ~ 0.5 μm diameter (Fig. 5b). These observations suggest that liquid eutectic carbonate salt be easily to penetrate into the non-sintered MgO substrate.

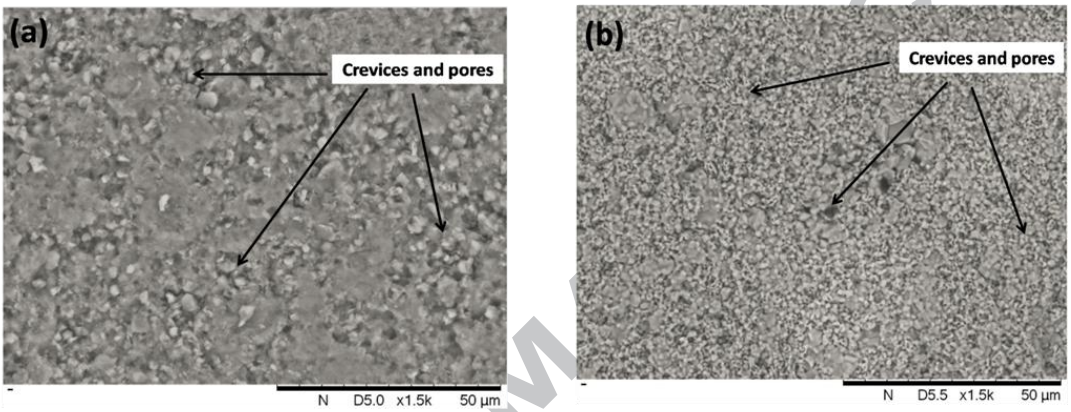

Fig. 5. SEM images of non-sintered MgO substrate (a) and the substrate sintered at 1100°C (b).

The above observations also agree with the following Washburn equation [15].

$$h^2 = \frac{r\sigma_{LV}cos\theta}{2\mu} \quad (2)$$

where r is the radius of capillary or pores, σ_{LV} is the surface tension, θ is the contact angle, μ is the viscosity and t is the time taken to reach an infiltration height of h. Equation 2 applies to cases of high wettability and acute contact angle, which is indeed the case for the eutectic carbonate salt on both sintered and non-sintered MgO substrates. Equation 2 also indicates that the infiltration of carbonate salt on non-sintered MgO

substrate should be more significant than that of the sintered MgO substrate due to the large pore sizes. This has been validated by the SEM-EDS analyses; see below.

Figs. 6 and 7 show the SEM-EDS images and analyses of the interface between the MgO substrates and the carbonate salt. Considerable salt infiltration into the MgO substrate is evident, particularly for the non-sintered MgO substrate (Fig. 6) where an infiltration depth of ~ 1.5 mm can be observed, significantly larger than that for the sintered MgO substrate (~ 0.5 mm, Fig. 7). Such a difference could be explained from two aspects: One is that the size and number of crevices and pores of non-sintered MgO substrate are larger than that of the sintered MgO substrate (Fig. 5); the other is that the specific structure of the sintered MgO substrate, which may hinder the salt penetration. As illustrated in Fig. 5b, the sintered MgO substrate is in the early stage of sintering process with individual particles visibly distinguishable and sintering necks likely starting to growth [16][17]. The sintering of MgO particles is likely to form a rigid microstructure that could confine the motion of liquid carbonate salt into the substrate.

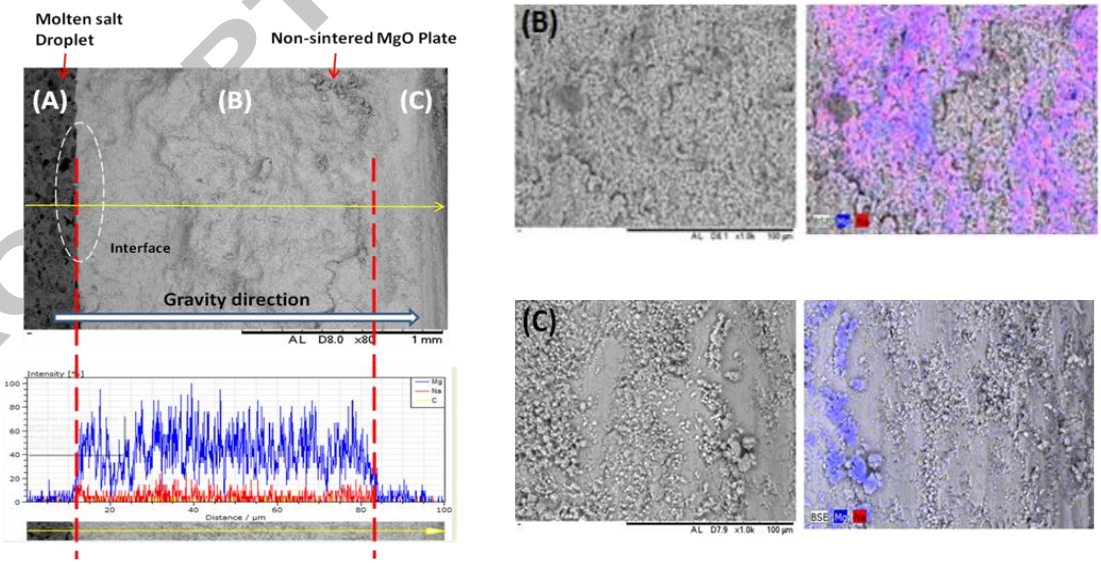

Fig. 6. SEM-EDS analyses of the interface between the carbonate salt and the non-sintered MgO substrate - (A): Carbonate salt droplet; (B) and (C): Non-sintered MgO substrate; Colors in EDS mapping: Red – Na; Blue – Mg.

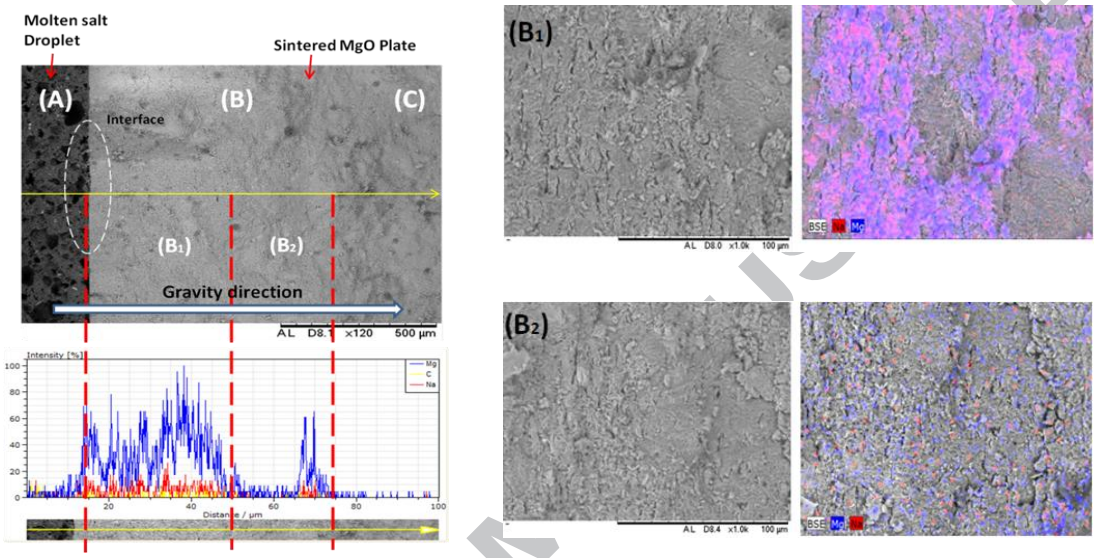

Fig. 7. SEM-EDS analyses of the interface between the carbonate salt and the sintered MgO substrate (sintered at 1100°C) - (A): Carbonate salt droplet; (B) and (C): Sintered MgO substrate; Colors in EDS mapping: Red – Na; Blue – Mg.

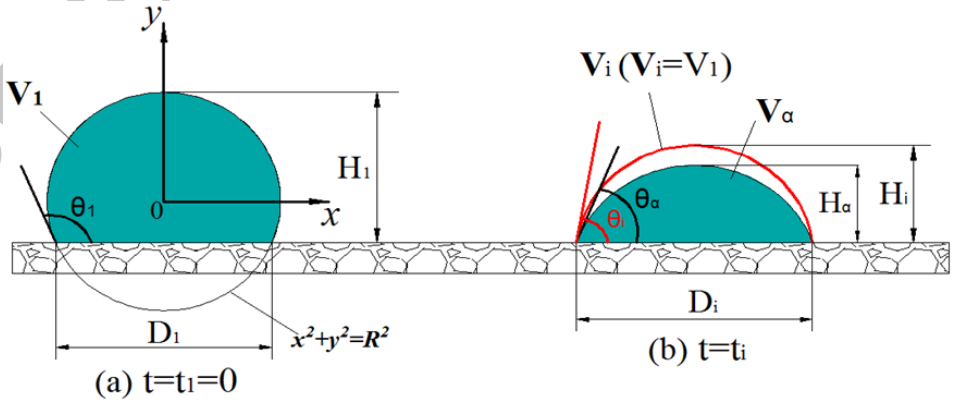

Fig. 8. Schematic illustration of changes of a carbonate salt droplet on an MgO substrate due to infiltration; Red line in (b) denotes the contour of salt droplet without infiltration.

As discussed earlier, the extent of salt infiltration increases with increasing wettability of the salt on the substrate, leading to a decrease in the droplet volume on the substrate, and hence influence on the measured contact angle. In other words, the actual contact angle is different from the measured value. Therefore, the effect of infiltration should be taken into consideration when studying this sort of liquid-substrate combination.

Quantification of the effect of salt infiltration on the contact angle could be evaluated by using the evaporation method proposed by Kondoh et al. [18]. For doing so, the salt droplet is assumed to be part of a sphere with radius *R* and the infiltration has no effect on the wetting experiments. Under those assumptions, the volume of salt droplet on the substrate should be constant and does not change with the time during experiments. This is illustrated in Fig. 8 where V, D, H and θ are respectively the salt droplet volume, droplet diameter, droplet height and contact angle; *t* is time; and subscript *1* and *i* represent respectively time=0 and *i*. D_i and H_α in Fig. 8b denote respectively the measured droplet diameter and height; whereas the red line in the figure denotes the droplet contour without the effect of infiltration, i.e. $V_i = V_1$. The contact angle at $t = 0$ and volume of the carbonate salt drop at any moment on the substrate ($V_i = V_1$) can be expressed by:

$$sin\theta_1 = \frac{D_1}{2R} \tag{3}$$

$$V_1 = \int_{-(H_1-R)}^{R} \pi(R^2-y^2)\,dy = \pi\left(\frac{D_1 H_1^2}{2sin\theta_1} - \frac{H_1^3}{3}\right) \tag{4}$$

where R represents the droplet radius. The change in the droplet height and radius, and the contact angle at any moment can then be calculated by:

$$H_i^3 + \frac{3D_i^2 H_i}{4} - \frac{6V_1}{\pi} = 0 \quad (5)$$

$$R_i = \frac{V_1}{\pi H_i^2} + \frac{H_i}{3} \quad (6)$$

$$\theta_i = sin^{-1} \frac{D_i}{2R_i} \quad (7)$$

Insertion of the experimentally measured D_i into Equations 5-7 gives the modified droplet height, radius and contact angle. Fig. 9 shows the modified contact angle on different MgO substrates (non-sintered, sintered and single crystal) taking into account of the salt penetration. As mentioned before, the use of single crystal MgO substrate is to show the result with no infiltration for comparative purpose. One can see significant effect of the substrate on the contact angle. For the non-penetration single crystal substrate, the wetting and spreading process is far quicker than that with other two substrates, giving the final equilibrium contact angle of 40°. The contact angle of the carbonate salt on the non-sintered MgO and sintered MgO substrates are respectively 25° and 32°, considerably lower than that for the single crystal MgO plate.

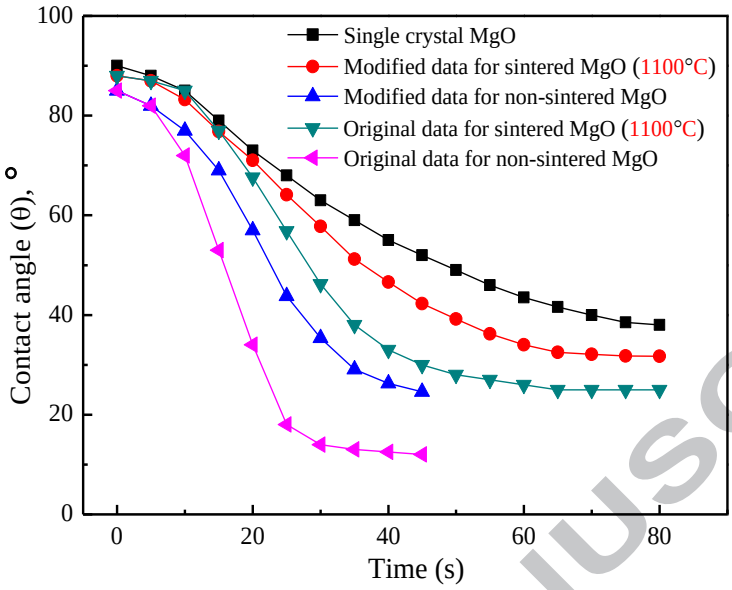

Fig. 9. Effect of substrate type on the contact angle.

3.4 Surface energy

The results presented in Section 3.2 suggest that the structure of the substrate plays an important role in the wetting and contact angle of the salt. The structure of the substrate very much depends on the sintering temperature should the substrate be made from powders - the cases of this study for both the sintered and non-sintered substrate. Single crystal MgO could also be made by sintering at very high temperature (~ 3000 ℃). Different substrate structures produced at different sintering temperatures could mean different surface energies. As a result, an attempt is made in the following to explain the experimental observations of wetting and contact angle from the view point of surface energy.

At equilibrium, the contact angle depends on interactions between different phases, and can be described by the Young's equation:

$$cos\theta = \frac{\sigma_{sv}-\sigma_{sl}}{\sigma_{lv}} \quad (8)$$

where σ_{lv}, σ_{sv} and σ_{sl} are respectively liquid-vapour, solid-vapour and solid-liquid interfacial tensions. For a given liquid phase, the eutectic carbonate salt of $NaLiCO_3$ in this study, σ_{lv} is constant, the difference between σ_{sv} and σ_{sl} is the only factor that determines the value of contact angle. Let σ be defined as the difference:

$$\sigma = \sigma_{sv} - \sigma_{sl} \quad (9)$$

In Equation 9, σ_{sv} depends on the intrinsic property of the substrate, whereas σ_{sl} is due to the interaction between the eutectic carbonate salt and the substrate. The interfacial tension could be linked to intermolecular forces and polarity of the phases. For example, σ_{sl} can be given by [19]:

$$\sigma_{sl} = \sigma_{sv} + \sigma_{lv} - 2(\sigma_{sv}^{d} \cdot \sigma_{lv}^{d})^{1/2} - 2(\sigma_{sv}^{p} \cdot \sigma_{lv}^{p})^{1/2} \quad (10)$$

where the superscripts d and p denote respectively the dispersion and polar contributions to the surface tension. In cases where only dispersion forces operate, the polar term goes and Equation 10 becomes the Fowkes equation [20]:

$$\sigma_{sl} = \sigma_{sv} + \sigma_{lv} - 2(\sigma_{sv}^{d} \cdot \sigma_{lv}^{d})^{1/2} \quad (11)$$

Inserting Equation 11 to Equation 9 yields:

$$\sigma = 2(\sigma_{sv}^{d} \cdot \sigma_{lv}^{d})^{1/2} - \sigma_{lv} \quad (12)$$

Equation 12 suggests that the interfacial tension difference, σ, be determined by σ_{sv} (interfacial tension between solid and vapor phases), given the liquid-vapor interfacial

tension (σ_{lv}). This implies that the contact angle depends on the interfacial energy between the vapour phase and the measured solid surface.

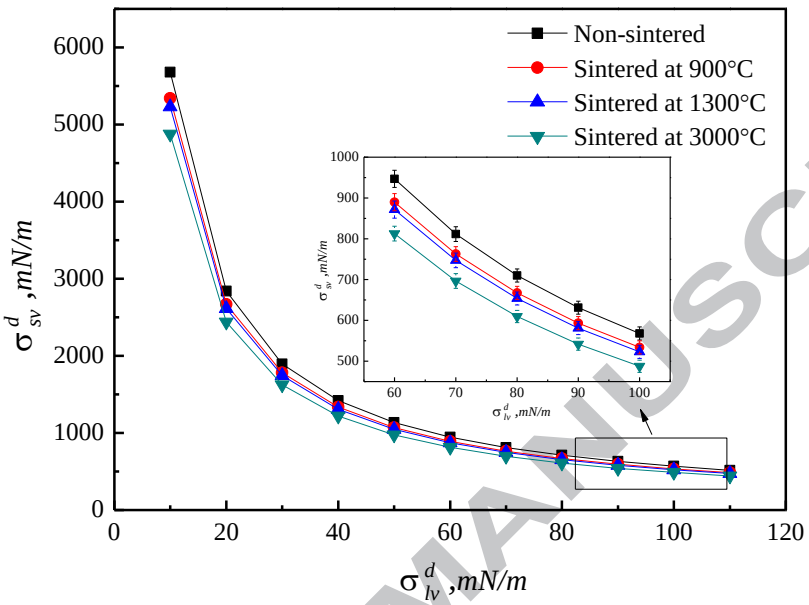

Fig. 10. Substrate surface tension vs molten salt surface tension for MgO substrate sintered at different temperatures.

Fig. 10 depicts the surface tensions of the substrates sintered at different temperatures as a function of the eutectic carbonate salt surface tension in which only dispersion interaction is considered. In the figure, the surface tension of $NaLiCO_3$, σ_{lv}, is taken as 250.039 mN/m [21]. One can see that the substrate surface tension decreases with an increase in the salt surface tension. For a given dispersive force of eutectic carbonate salt, the dispersive force of the MgO substrate decreases with increasing sintering temperature of substrate (3000^{o}C sintering temperature denotes single crystal MgO). The salt on the non-sintered MgO substrate has the smallest contact angle as demonstrated before,

indicating the greatest the substrate surface tension. This is exactly what we observed experimentally. This is also explains that the single crystal MgO substrate give the lowest surface tension. The above results also indicate that the sintering temperature plays an important role due to its effect on the structure of the substrate. To further investigate this effect, AFM analyses on the MgO substrates were carried out by using a Nanoscope III AFM with functionalised silica tips from Mikromasch (USA). The measurements were done mainly on the adhesion force and the principle of the measurements has been described elsewhere in the literatures [22][23]. Briefly, an AFM measures the cantilever deflection of the tip displacement due to its interaction with the substrate. The adhesion force can be calculated from the Hooke's law [24]:

$$F = k\Delta\varepsilon \tag{13}$$

where k is the spring constant of the cantilever calculated to be 0.179 N/m and $\Delta\varepsilon$ is the maximum cantilever deflection. Fig. 11 shows the measured force-displacement curves for the three MgO substrates. The insert in Fig. 11 gives the adhesion forces for the three substrates. One can see that the single crystal MgO substrate gives an adhesion force of 2.1 nN. Significantly larger adhesion forces are observed for both the sintered and non-sintered MgO substrates, with that for the non-sintered MgO substrate (~8.4 nN) nearly 2.5 times that for the sintered MgO substrate (~3.5 nN). The significant difference in the adhesion forces for the three substrates indicates the effect of different surface microstructure.

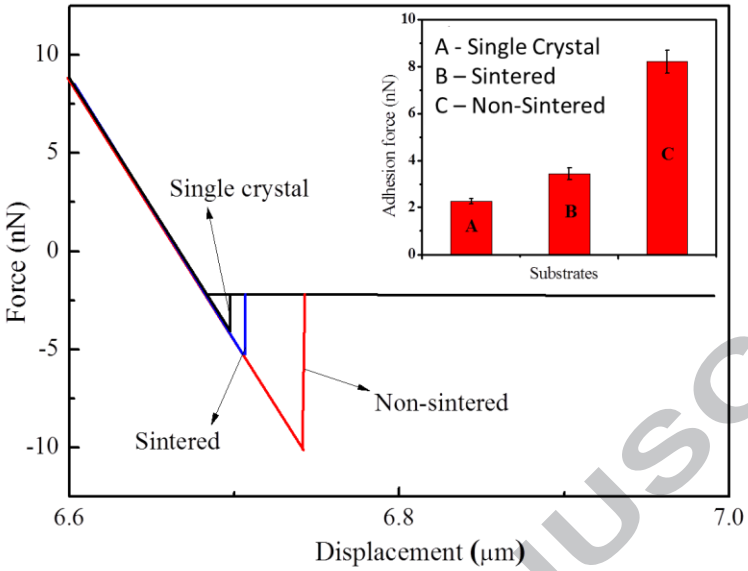

Fig. 11. Typical force-displacement curves for the three MgO substrates. The inset summarizes the average adhesion force for three MgO substrates.

The adhesion force between the tip and the substrate is the sum of several forces and can be expressed by [20]:

$$F = F_{el} + F_{vdw} + F_{cap} + F_{chem} \tag{14}$$

where F_{el}, F_{vdw}, F_{cap} and F_{chem} represent respectively the electrostatic force, Van der Waals force, meniscus or capillary force and chemical bond or acid-base interacting force. Under the ambient conditions, the dominant adhesion force is the capillary force due to the formation of a liquid meniscus between the tip and the substrate. Assuming that the AFM tip is a hemisphere with radius R_t in contact with the substrate, and liquid volume is negligible, the capillary force can be given by [24]:

$$F_{cap} = 2\pi\gamma_{lv}R_t(cos\theta_1 + cos\theta_2) \tag{15}$$

where γ_{lv} is the surface tension at the liquid vapour interface, and θ_1 and θ_2 are the contact angles between the liquid and the tip, and the liquid and the substrate, respectively. Insertion of the Equation 15 into Equations 13 and 14 gives the contact angle of liquid and the substrate as:

$$cos\theta_2 = \frac{kx}{2\pi\gamma_{lv}R_t} - cos\theta_1 \quad (16)$$

Equation 16 shows that the contact angle of the liquid and the substrate depends on the adhesion force; the larger the adhesion force, the smaller the contact angle. Equations 14-16 also indicate that the non-sintered MgO substrate has the highest surface tension in agreement with experimental observations discussed above. As mentioned previously, sintering temperature determines the microstructure of the MgO substrate given other conditions, and hence the surface energy and contact angle upon in contact with the salt. More experiments were then carried out on the MgO substrates sintered at different temperatures. Table 2 summarizes the results. For comparison, the result for the single crystal MgO (denoted as sintered at 3000 ℃) is also included. One can see that when the sintering temperature increases from 500 ℃ to 3000 ℃, the contact angle increases from 25° to 40°.

Table 2

Contact angle of the carbonate salt on MgO substrates sintered at different temperatures

Sintering temperature (℃)	500	700	900	1100	1300	3000
Contact angle	25° (±1.7°)	25°(±1.8°)	32°(±1.6°)	32°(±1.8°)	34°(±1.7°)	40°(±1.8°)

4. Conclusions

The wetting behavior of a eutectic carbonate salt of $NaLiCO_3$ on MgO substrate has been investigated through contact angle measurements at an elevated temperature of 778K. Both non-sintered and sintered MgO substrates were prepared for the study. For the sintered substrates, different sintering temperatures were used to obtain different substrate structure. For comparison purposes, a single crystal MgO substrate was also used in the study. To accounting for the effect of salt penetration into the substrate, a calculation model was used to obtain the true contact angle value. The results show good wettability of the carbonate salt on the MgO substrates and the wettability is a fairly strong function of surface structure and hence surface energy of the MgO substrates obtained using different sintering temperature. The non-sintered MgO substrate has a loose surface particle packing with large pores and crevices, leading to significant salt infiltration. The corresponding contact angle is measured to be 25°. The structure and morphology of sintered MgO substrates depend the sintering temperature given other conditions, the higher the sintering temperature, the finer the particles on the surface, the more homogenous the particle distribution, and the smaller the size of the porous and crevices on the substrate surface. The contact angle of the salt on the sintered MgO increases with increasing temperature of the MgO substrate preparation and approaches ~40° for the single MgO crystal. The effect of the sintering temperature for making the MgO substrate could be linked to the surface energy, and the linkage is validated by the AFM measurements of the adhesion forces of the MgO substrates. These findings indicate a direct linkage between the substrate structure and the surface wettability, which could be

used to guide the engineering of composite thermal energy storage materials for an optimal combination of mechanical and thermosphysical properties.

The wetting behavior of a eutectic carbonate salt of $NaLiCO_3$ on MgO substrate has been investigated through contact angle measurements at an elevated temperature of 778K. Both non-sintered and sintered MgO substrates were prepared for the study. For the sintered substrates, different sintering temperatures were used to obtain different substrate structures. For comparison purposes, a single crystal MgO substrate was also used in the work. The influences of two factors on the contact angle were studied: (a) penetration of carbonate salt into MgO substrate, and (b) surface tension changes due to different fabrication temperatures of the substrates. On the basis of experimental observations and theoretical analyses, the following conclusions could be made:

(1). Good wettability of the eutectic carbonate salt on the MgO substrates is observed and the wettability is a fairly strong function of surface structure and hence surface energy of the MgO substrates.

(2). The non-sintered MgO substrate has a loose surface particle packing with large pores and crevices, leading to significant salt infiltration, and the corresponding measured contact angle of 25°.

(3). The contact angle of the salt on the sintered MgO increases with increasing temperature of the MgO substrate preparation and approaches ~40° for the single MgO crystal.

(4). The effect of sintering temperature for making the MgO substrate could be linked to the surface energy and the surface energy of the MgO substrate decreases with increasing

sintering temperature of the substrate, indicating a direct linkage between the substrate structure and the surface wettability.

Acknowledgements

This research is supported by the UK Engineering and Physical Sciences Research Council (EPSRC) under grants EP/P004709/1, EP/P003435/1, EP/L019469/1, EP/F060955/1, EP/L014211/1 and EP/K002252/1, the British Council under 2016-RLWK7-10243, China Scholarship Council (CSC), and a USTB grant for UoB-USTB joint Centre.

References

[1] I. Gur, K. Sawyer, R. Prasher. Engineering. Searching for a better thermal battery. Science 335 (2012) 1454-1455.

[2] Joseph P. Heremans. Thermoelectricity: The ugly duckling. Nature 508 (2014) 327-328.

[3] Sarada Kuravi, Jamie Trahan, D. Yogi GOswami, Muhammed M. Rahman, Elia K. Stefanakos. Thermal energy storage technologies and systems for concentrating solar power plants. Prog. Energy Combust. Sci. 39 (2013) 285-319.

[4] Dan Nchelatebe Nkwetta, Fariborz Hagighat. Thermal energy storage with phase change material—A state-of-the art review. Sustain. Cities Soc. 10 (2014) 87-100.

[5] Zhiwei Ge, Yongliang Li, Dacheng Li, Ze Sun, Yi Jin, Chuanping Liu, Chuan Li, Guanghui Leng, Yulong Ding. Thermal energy storage: Challenges and the role of particle technology. Particuology 15 (2014) 2-8.

[6] Zhiwei Ge, Feng Ye, Yulong Ding. Composite materials for thermal energy storage: Enhancing performance through microstructures. ChemSusChem 7 (2014) 1318-1325.

[7] Zhiwei Ge, Feng Ye, Hui Cao, Guanghui Leng, Yue Qin, Yulong Ding. Carbonate-salt-based composite materials for medium and high temperature thermal energy storage. Particuology 15 (2014) 77-81.

[8] Keping Chen, Xuejiang Yu, Chunrong Tian, Jianhua Wang. Preparation and characterization of form-stable paraffin/polyurethane composites as phase change materials for thermal energy storage. Energy Convers. Manage. 77 (2014) 13-21.

[9] Mohammad Mehrali, Sara Tahan Latibari, Mehdi Mehrali, Teuku Meurah Indra Mahlia, Hendrik Simon Cornrils Metselaar. Preparation and characterization of palmitic acid/grapheme nanoplatelets composite with remarkable thermal conductivity as a novel shape-stabilized phase change material. Appl. Therm. Eng. 61 (2013) 633-640.

[10] Murat M Kenisarin. High-temperature phase change materials for thermal energy storage. Renewable Sustainable Energy Rev. 14 (2010) 955-970.

[11] Feng Ye, Zhiwei Ge, Yulong Ding, Jun Yang. Multi-walled carbon nanotubes added to Na_2CO_3/MgO composites forthermal energy storage. Particuology 15 (2014) 56-60.

[12] Moran Wang, Ning Pan. Predictions of effective physical properties of complex multiphase materials. Mater. Sci. Eng., R 63 (2008) 1-30.

[13] Likun Zang, Zhangfu Yuan, Hongxin Zhao, Xiaorui Zhang. Wettability of molten Sn-Bi-Cu solder on Cu substrate. Mater. Lett. 63 (2009) 2067-2069.

[14] R.N. Wenzel. Resistance of solid surfaces to wetting by water. Ind. Eng. Chem. 28 (7) (1936) 988-994.

[15] Longlong Yang, Ping Shen, Qiaoli Lin, Feng Qiu, Qichuan Jiang. Wetting of porous graphite by Cu-Ti alloys at 1373 K. Mater. Chem. Phys. 124 (2010) 499-503.

[16] F.B. Swinkel, M.F. Ashby. A second report on sintering diagrams. Acta Metall. 29 (1981) 259-281.

[17] M.F. Ashby. A first report on sintering diagrams. Acta Metall. 22 (1974) 275-289.

[18] Katsuyoshi Kondoh, Masashi Kawakami, Hisashi Imai, Junko Umeda, Hidetoshi Fujii. Wettability of pure Ti by molten pure Mg droplets. Acta Mater. 58 (2010) 606-614.

[19] Carmen Chiappoori, Saverio Russo, Antonio Turturro. Wettability of glass substrates by molten nylon-6. Polymer 22 (1981) 534-538.

[20] B.S. Tanem, O. Lunder, A. Borg, J. Mardalen. AFM adhesion force measurements on conversion-coated EN AW-6082-T6 aluminium. Int. J. Adhes. Adhes. 29 (2009) 471-477.

[21] George J. Janz. Thermodynamic and transport properties for molten salts: Correction equations for critically evaluated density, surface tension, electrical conductance, and viscosity data. J. Phys. Chem. Ref. Data 17 (2) (1988) 1-309.

[22] Stephan Frybort, Michael Obersriebnig, Ulrich Muller, Wolfgang Gindl-Altmutter, Johannes Konnerth. Variability in surface polarity of wood by means of AFM adhesionforce mapping. Colloids Surf., A 457 (2014) 82-87.

[23] M. Meincken, T.A. Berhane, P.E. Mallon. Tracking the hydrophobicity recovery of PDMS compounds using the adhesive force determined by AFM force distance measurements. Polymer 46 (2005) 203-208.

[24] IM Pelin, A Piednoir, D Machon, P Farge, C Pirat, SM Ramos. Adhesion forces between AFM tips and superficial dentin surfaces. J. Colloid Interface Sci. 376 (2012) 262-268.

Graphical abstract

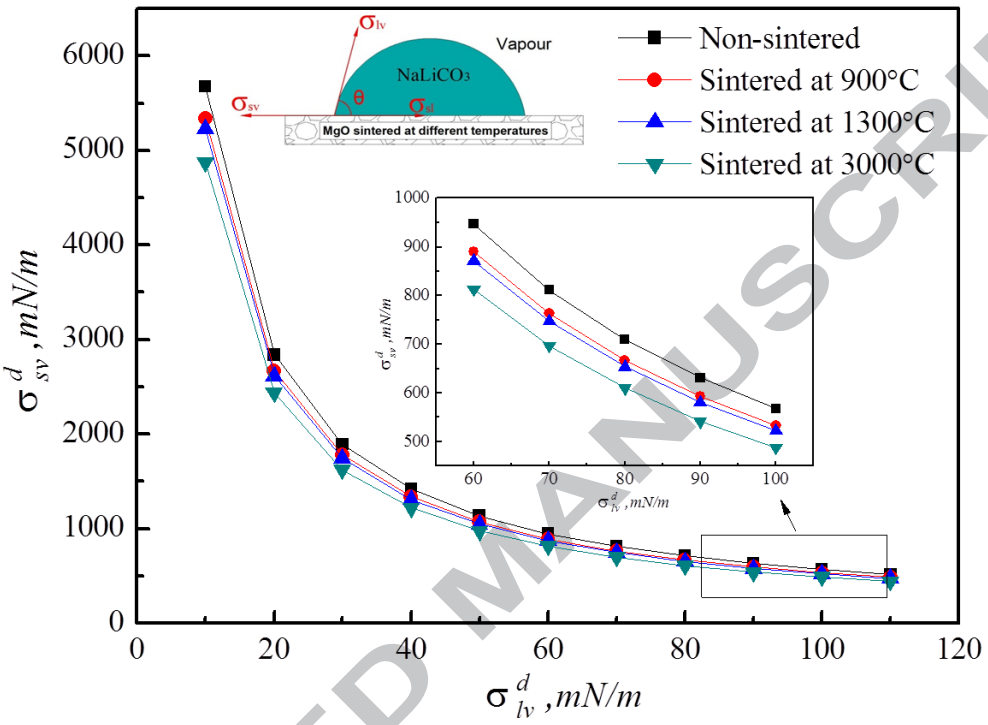

Highlights

- The wettability behaviour of carbonate salt on MgO was investigated through contact angle measurements.
- Good wettability of the carbonate salt on both the non-sintered and sintered MgO substrates was observed.
- The contact angle of the salt on the sintered MgO increases with increasing sintering temperature of the MgO substrate fabrication.
- The wettability is a fairly strong function of microstructure and hence surface energy of the MgO substrates obtained using different sintering temperature.